Computers & Geosciences 133 (2019) 104316

Contents lists available at ScienceDirect

Computers and Geosciences

journal homepage: www.elsevier.com/locate/cageo

A library of BASIC scripts of reaction rates for geochemical modeling using PHREEQC

Yilun Zhang [a,c,1], Bin Hu [b,1], Yanguo Teng [b], Kevin Tu [d], Chen Zhu [a,*]

[a] Department of Earth and Atmospheric Sciences, Indiana University, Bloomington, IN, 47405, USA
[b] College of Water Sciences, Beijing Normal University, Beijing, 100875, China
[c] Doctoral program in environmental sciences, Indiana University, Bloomington, IN, 47405, USA
[d] School of Informatics and Computer Sciences, Indiana University, Bloomington, IN, 47405, USA

ARTICLE INFO

Keywords:
PHREEQC
Kinetics
Rate equations
Geochemical modeling

ABSTRACT

Rate equations and kinetic parameters for about 100 minerals were programmed into a library of callable Basic language scripts for the geochemical modeling program PHREEQC (version 3.5.0) to facilitate the application of kinetics in geochemical modeling. For most minerals, the following general equation is used: r_{net} $S_A \sum_j A_j e^{E_{a_j} RT} \prod_i a_{ij}^{ni} 1 \quad \Omega^{p_j} {}^{q_j}$

where r_{net} stands for the net dissolution rate of a mineral phase (mol kgw ^{1} s ^{1}); j the jth reaction mechanism; S_A the surface area per unit water mass (m^2 kgw ^{1}); A_j the Arrhenius pre-exponential factor (mol m ^{2} s ^{1}); $E_{a,j}$ the apparent reaction activation energy (J mol ^{1}); R the universal gas constant (8.31446 J mol ^{1} K ^{1}); T the temperature (K); a_i the activity of aqueous species i; the mineral saturation quotient. p_j and q_j are empirical fitting parameters. j stands for the specific mechanisms of reaction. Other forms of rate equations and associated parameters programmed in the library include parallel mechanisms, Langmuir adsorption isotherm, and empirical rate equations that apply to a specific reaction mechanism or geochemical system. A separate file of PHASEs, which define the chemical stoichiometry of the phases, dissolution reactions, and equilibrium constants of the dissolution reactions, is also provided. PHREEQC requires that the names in PHASES and RATES blocks match with each other.

The Basic language scripts can also be used as templates for writing other rate equations which users might wish to use. To illustrate the application of the script library, we simulated the reaction path of albite dissolution at 25 C and 1 bar, using three rate equations and compared the results. The script and phase library and supporting materials can be downloaded from https://github.com/HydrogeoIU/PHREEQC-Kinetic-Library and doi.org/10.5967/41gq-yr13.

1. Introduction

In the last three decades, a large number of laboratory experiments have produced mineral dissolution rates in a wide range of temperatures, pH, and solution chemistry (see reviews by Brantley et al., 2008, pp. 151 210; Marini, 2007, pp. 211 266; Palandri and Kharaka, 2004; Schott et al., 2009). As a result, applications of reaction kinetics to water-rock interaction have also grown significantly in such fields as carbon dioxide sequestration (e.g., Knauss et al., 2005; Liu et al., 2011, 2012; Lu et al., 2011, 2013; 2015; Tutolo et al., 2015; White et al., 2005; Wilkin and DiGiulio, 2010; Xu et al., 2007; Xu et al., 2010; Zhang et al., 2013; Zhang et al., 2015; Zhang et al., 2016), diagenetic processes (Jones and Xiao, 2005, 2006; Lu and Cantrell, 2016; Roy et al., 2011; Whitaker and Xiao, 2010), geothermal systems (Dobson et al., 2004; Giambalvo et al., 2002; Spycher et al., 2003; Wanner et al., 2014; Xu and Pruess, 2001; Xu et al., 2004), and weathering (Maher et al., 2009; Perez-Fodich and Derry, 2019). Furthermore, advances in geochemical modeling software development have made application of kinetics to geochemical models much easier (Parkhurst and Appelo, 2013). Using thermodynamic data (e.g., equilibrium constants and activity coefficient models) and kinetic parameters (e.g., rate constants and activation energy), mineral dissolution and precipitation processes can be quantified

* Corresponding author.
E-mail address: chenzhu@indiana.edu (C. Zhu).
[1] These authors contributed equally to this work.

https://doi.org/10.1016/j.cageo.2019.104316
Received 13 December 2018; Received in revised form 6 August 2019; Accepted 23 August 2019
Available online 29 August 2019

with geochemical modeling software (e.g., EQ3/6: Wolery, 1992; PHREEQC: Parkhurst and Appelo, 1999, 2013; ToughReact: Xu et al., 2006, 2011; Crunchflow, Steefel et al., 2015).

Among the many geochemical simulation programs, the software package PHREEQC a computer program for simulating aqueous speciation, reaction path, and 1-D reactive transport (Charlton and Parkhurst, 2011; Parkhurst and Appelo, 2013) has gained popularity. This is partly because the program allows the user to describe the rate equations via BASIC scripts. These scripts are then run with the program along with other parts of input files and databases for kinetic model simulations. For example, Zhu et al. (2010) constructed a reaction path model for feldspar dissolution and secondary mineral precipitation in batch systems with their own PHREEQC database and kinetics scripts. Geochemical models of fluid-rock interaction have evolved from equilibrium only to kinetic approaches, thus addressing geochemical reactions on a real time scale (Zhu, 2009).

However, the databases that accompany the PHREEQC package only contain limited rate equations. Much of the kinetics data needed for geochemical modeling is scattered in the literature. Proper assembly of the kinetic data needed for modeling, such as preparing the codes for kinetic scripts and assembling other necessary parts for kinetic calculation, is an intimidating task for many users. To facilitate the use of kinetics in geochemical modeling, we collected the rate equations and kinetic parameters from the literature and compiled them into a library of scripts for PHREEQC. These BASIC language data blocks can be readily copied into input files or databases.

It is beyond the scope of this study to evaluate kinetic experiments and compile them into an internally consistent kinetic database. In fact, we took the kinetic parameters from the literature directly as they are and programmed them in easy-to-use formats. In this sense, users must be very careful about the conditions of these kinetic parameters are applicable. These conditions include the temperature, pH, solution chemistry, and saturation states. As they are in the original sources, the kinetic parameters for most minerals in this library were derived from dissolution experiments at far-from-equilibrium conditions. Extrapolation of them to near-equilibrium and precipitation conditions need careful verification. Users must be aware of this and other assumptions when applying this kinetic library to systems beyond the experimental conditions in the original studies.

The resulting library contains kinetic data for approximately 100 minerals. We understand that to derive a comprehensive and self-consistent kinetic rate database is a daunting task, and this library represents only the first effort in a long, multiphase project. The script and phase library and supporting materials can be downloaded from https://github.com/HydrogeoIU/PHREEQC-Kinetic-Library and doi.org/10.5967/41gq-yr13. The library of scripts are also included in an online version of PHREEQC, which can be accessed at the corresponding author s Indiana University web site www.hydrogeochem.earth.indiana.edu.

2. RATES and RATE equations

2.1. General expression of rates and rate equations

The readers are referred to the textbooks by Lasaga (1998), Marini (2007), Brantley et al. (2008), and Rimstidt (2014) for the background of geochemical kinetics. Here we only briefly introduce necessary background for presenting the kinetic library.

Geochemical reaction rates can be defined as the change of concentration of reactants and products with time over the course of a chemical reaction (Rimstidt, 2014, pp. 36 39; Zhu and Anderson, 2002):

$$r_{net} \quad \frac{1}{v_i}\frac{dC_i}{dt} \tag{1}$$

where r_{net} denotes net or overall mineral dissolution or destruction rate (mol kgw ^{1} s ^{1}), C_i is the concentration of a reactant or product (mol kgw ^{1}), t is the time (s), and v_i is the stoichiometry coefficient of reactant or product i in this reaction (see Table 1 for all symbols and notations). In this paper, we followed the convention that positive values of r represent dissolution rates whereas negative values represent the precipitation rates. Note that PHREEQC calculation is based on water mass, the unit of the reacting mineral phases are mol kgw ^{1}. 1 mol kgw ^{1} means 1 mol of this mineral phase is contacted and reacting with 1 kg of solution.

Table 1
List of symbols and definitions.

Symbol	Definition
A	Arrhenius pre-exponential factor (mol m ^{2} s ^{1})
a_i	Activity of species i
c_i	Molality of species i (mol kgw ^{1})
E_a	Apparent reaction activation energy (J mol ^{1})
$_rG$	Gibbs free energy of the dissolution reaction,
J	Dissolution flux (mol m ^{2} s ^{1})
K	Equilibrium constant
k	Rate constant (mol m ^{2} s ^{1})
k'	Rate coefficient (s ^{1})
m	Current moles of minerals per water mass (mol kgw ^{1})
m_0	Initial moles of minerals per water mass (mol kgw ^{1})
n_i	Reaction order for species i
p, q	Empirical exponents
Q	Reaction quotient
R	Universal gas constant (8.31446 J mol ^{1} K ^{1})
r	Reaction rate of mineral (mol kgw ^{1} s ^{1})
r_j	Reaction rate of mineral for mechanism j (mol kgw ^{1} s ^{1})
S_A	Surface area per unit water mass (m ^{2} kgw ^{1})
S_A	Initial surface area per unit water mass (m ^{2} kgw ^{1})
SI	Mineral saturation index (log)
T	Temperature (K)
t	Time (s)
β_1, β_2	Correction parameters
v_i	Stoichiometry coefficient of reactant or product i in the reaction
ρ	Density of reactive surface sites on the mineral surface (mol m ^{2})
	Mineral saturation quotient (Q/K)

A rate law is an equation that relates the reaction rate to the concentrations of the participating species and other environmental conditions (Zhu and Anderson, 2002). Let us start with a general expression of the reaction rate (e.g., Lasaga, 1998, pp. 186 191):

$$r_{net} \quad S_A \sum_j A_j e^{\ E_{a\,j}\ \ RT} \prod_i a_{i\,j}^{ni} f\ \ \Delta_r G \tag{2}$$

where j stands for a specific mechanism of reaction, such as proton catalyzed dissolution; S_A the surface area per unit water mass (m^2 kgw ^{1}); A_j the Arrhenius pre-exponential factor for the jth mechanism (mol m ^{2} s ^{1}); $E_{a,j}$ the apparent reaction activation energy (J mol ^{1}) for the jth mechanism; R the universal gas constant (8.31446 J mol ^{1} K ^{1}); T the temperature (K); a_i the activity of aqueous species i that catalyze or inhibits the jth mechanism. f $_rG$ denotes rate dependence as a function of the Gibbs free energy of a dissolution reaction. Below, we will elaborate on each term in Eqn (2).

2.2. Rate dependence on pH

The pH has a significant effect on the reaction rate for most minerals. Palandri and Kharaka (2004) modeled the pH-dependence of reaction rates by dividing the dissolution process into three mechanisms: H , H_2O, and OH -promoted mechanisms, which they assume operate in the ranges of pH 1.3 4.0, 5.6 8.2, and 8.6 10.3, respectively. If we assume these three are the only mechanisms for the reactions and for the moment, only wish to deal with forward rates r , not net rates, Eqn (2) becomes,

$$r \quad r_{H} \quad r_{w} \quad r_{OH} \tag{3}$$

where H, w, and OH denote to the acid, neutral, and basic mechanism, respectively.

Palandri and Kharaka (2004) carried out piecewise linear regression of the experimental rate data through the equations,

$$r_{+,H} = A_H a_{H^+}^{n_H} e^{-E_{a,H}/RT} \quad (4a)$$

$$r_{+,w} = A_w e^{-E_{a,w}/RT} \quad (4b)$$

$$r_{+,OH} = A_{OH} a_{H^+}^{n_{OH}} e^{-E_{a,OH}/RT} \quad (4c)$$

The logarithm form transforms Eqn (4) into a linear relation,

$$\log(r_{+,H}) = \log(A_H) - E_{a,H}/2.303RT + n_H pH \quad (5a)$$

$$\log(r_{+,w}) = \log(A_w) - E_{a,w}/2.303RT \quad (5b)$$

$$\log(r_{+,OH}) = \log(A_{OH}) - E_{a,OH}/2.303RT + n_{OH} pH \quad (5c)$$

where n_H and n_{OH} are reaction orders of the H^+ in acid and base mechanisms, respectively.

These kinetic parameters A_H, A_w, A_{OH}, n_H, n_{OH}, $E_{a,H}$, $E_{a,w}$, and $E_{a,OH}$, which describe the pH dependence, are programmed into the library and are also listed in Appendix A. Note that the pre-exponential factor is related to the apparent rate constant $k_{H,25}$ through the equation,

$$\log(k_{+H,25}) = \log(A_H) - \frac{E_{a,H}}{2.303RT} \quad (6)$$

where 25 denotes 25 °C (the reference state) and T is 298.15 in Eq. (6). $k_{+,H}$, $k_{+,w}$, and $k_{+,OH}$ at 25 °C are also listed in Appendix A.

2.3. Effect of temperature on rates

The reaction rate dependence on temperature can be described by the Arrhenius equation (Eq. (7)). This temperature effect is included in the scripts when apparent activation energy data for the minerals are available.

$$k_j = A_j e^{-E_{a,j}/RT} \quad (7)$$

The apparent activation energy for the dissolution reactions are also listed in Appendix A.

2.4. The surface area term

The term S_A in Eq. (2) stands for the reactive surface area (Helgeson et al., 1984) or the concentration of the reactive surface sites (Stumm, 1992). However, in practice, these properties are currently inaccessible, and S_A is approximated by either the BET or geometric surface areas. Most rate constants compiled from publications are largely normalized to BET surface areas. When applying the BET surface area-normalized rates in the library (from laboratory experiments) to field systems for which only geometric surface areas are available, a roughness factor of ~5–~7 may be warranted. This can be accomplished by including a scaling factor as PARM(2).

The surface area of the reacting phase may change as reaction proceeds. If the mineral particles have a spherical or cubic shape and dissolution proceeds uniformly, the changes of surface area during the reaction is approximated by the equation,

$$S_A = S_A^\circ \cdot \left(\frac{m}{m_0}\right)^{2/3} \quad (8)$$

On the other hand, when simulating precipitation, the surface area of the precipitating mineral is typically difficult to evaluate. Since all rate equations require a non-zero surface area to calculate the precipitation rate, the following assumptions are used in the scripts. If the initial mass of the precipitating phase is not 0 ($m_0 > 0$), the surface area for the precipitant is calculated using Eq. (8). If the initial mass of the precipitant is 0 ($m_0 = 0$), the surface area of precipitant is assumed to be constant over time. If no initial surface area is provided (i.e. $S_A^\circ \leq 0$), a default value of 1 $m^2\,kgw^{-1}$ for S_A° is to be used, allowing the calculation of precipitation rates and to avoid calculation error in the program.

2.5. Effect of saturation state on reaction rate

The term $f(\Delta_r G)$ in Eq. (2) is used to account for the relationship between the net reaction rates and the departure from equilibrium. Theoretically, $r_{net} = 0$ when $f(\Delta_r G) = 0$. One of the commonly used expressions for $f(\Delta_r G)$ is given by Eq. (9) (Alekseyev et al., 1997; Brantley et al., 2008, pp. 151–210; Lasaga, 1995, 1998; Lasaga et al., 1994; Oelkers et al., 1994):

$$f(\Delta_r G) = (1 - \Omega^p)^q = (1 - [Q/K]^p)^q = 1 - \left[e^{\Delta_r G/RT}\right]^p)^q \quad (9)$$

where Ω is the mineral saturation quotient, Q the reaction quotient, and K the equilibrium constant. The two dimensionless fitting parameters, p and q, are usually empirical.

When both p and q are equal to 1,

$$f(\Delta_r G) = (1 - \Omega) \quad (10)$$

and Eq. (2) reduces to Eq. (11) for reactions that do not involve a catalyst or inhibitor,

$$r_{net} = S_A \sum_j k_{+j}(1 - \Omega) \quad (11)$$

Eqs. (10) and (11) is often called the "transition state theory (TST) rate law" in the geochemistry literature. This is the default relationship used in the Palandri and Kharaka (2004) database when near-equilibrium experimental data are not available.

There are only a small number of near-equilibrium laboratory experiments available that allow regression of p and q values (Palandri and Kharaka, 2004; Marty et al., 2015). For most minerals in these databases or this library, no near-equilibrium experimental data are available for obtaining the p and q values. The ongoing practice is to assume that p and q values equal to 1 (Palandri and Kharaka, 2004; Marty et al., 2015). However, there is little experimental evidence that supports the validity of Eq. (11) for the geochemical reactions listed in the kinetics library. First, Eq. (11) is only valid for elementary reactions; geochemical reactions listed in the kinetics library are mostly overall reactions. For operational purposes, however, we must introduce a provisional $f(\Delta_r G)$ term in rate equations so that the net reaction rates go to zero at equilibrium. Therefore, Eq. (10) was used as default relationship for all RATES scripts that do not have p and q values. Users of the library should also note that most geochemical systems quickly depart from the initial far-from-equilibrium condition and approach to the near equilibrium region (Zhu et al., 2010). In other words, most reactions proceed in the near-equilibrium region where there are no experimental data available.

Another consequence of the *ad hoc* use of Eqs. (10) and (11) is that the scripts programmed with this relationship will automatically calculate precipitation when $\Delta_r G > 0$. However, there is a paucity of experimental precipitation rate data. As a result, Palandri and Kharaka (2004) had to invoke the principle of microscopic reversibility for most minerals—that is, to use the equilibrium constants (K) and forward rate constants (k_+) to calculate the rate constants of the reverse reactions (k_-). This principle, again, is only applicable for elementary reactions. Users must examine the relevant rate equations and may want to experiment with different rate equations for precipitation, such as the BCF equation (Pham et al., 2011).

To accommodate the experimental results that deviate from Eq. (11), more complicated empirical relationships for $f(\Delta_r G)$ have been proposed (Burch et al., 1993; Cappelli et al., 2018; Hellmann and Tisserand, 2006). These equations for $f(\Delta_r G)$ are also programmed into BASIC

```
############
#Quartz
############
quartz
-start
1 rem unit should be mol,kgw-1 and second-1
2 rem parm(1) is surface area in the unit of m2/kgw
3 rem calculation of surface area can be found in the note
4 rem M is current moles of minerals M0 is the initial moles of minerals
5 rem parm(2) is a correction factor
10 rem acid solution parameters
11 a1=0
12 E1=0
13 n1=0
20 rem neutral solution parameters
21 a2=1.98
22 E2=77000
30 rem basic solution parameters
31 a3=1.97E+04
32 E3=80000
33 n2=0.34
36 rem rate=0 if no mineral mass and undersaturated
40 SR_mineral=SR("quartz")
41 if (M<0) then goto 200
42 if (M=0 and SR_mineral<1) then goto 200
43 if (M0<=0) then SA=PARM(1) else SA=PARM(1)*(M/M0)^0.67
50 if (SA<=0) then SA=1
60 R=8.31451
75 Rate1=a1*EXP(-E1/R/TK)*ACT("H+")^n1  #acid rate expression
80 Rate2=a2*EXP(-E2/R/TK)               #neutral rate expression
85 Rate3=a3*EXP(-E3/R/TK)*ACT("OH-")^n2    #base rate expression
90 Rate=(Rate1+Rate2+Rate3)*(1-Sr_mineral)*SA*parm(2)
100 moles= rate*Time
200 save moles
-end
```

Fig. 1. An example kinetic script for quartz. The kinetic parameters and rate equation are from Palandri and Kharaka (2004).

scripts for dissolution range ($_rG$ 0). However, these empirical rate equations will lead to mathematical errors when directly applying to precipitation range where $_rG$ 0. Therefore, we programmed Eq. (11) into the scripts for precipitation condition if it is encountered during the model calculation.

Users of this kinetics library must be aware the operational nature of the scripts. The addition of Eq. (11) into the scripts intends to force the rate to be zero at equilibrium. It does not mean an endorsement of this rate and f $_rG$ relationship. Eq. (11) in the scripts will lead to precipitation of phases when $_rG$ 0. However, there is little experimental data on precipitation rates or rate equations. It is always the users who produce geochemical modeling results. Not the program or the kinetics library.

2.6. Other reaction mechanisms

Besides the acid, neutral, and basic mechanisms, other aqueous species may also participate in the reactions and affect the rates. For example, the dissolution rate of carbonate minerals is strongly related to the partial pressure of CO_2, which is in equilibrium with the solution (Plummer et al., 1978), and quartz dissolution can be facilitated by hydrofluoric acid (Mitra and Rimstidt, 2009). These effects are regarded as additional reaction mechanisms and the rate can be expressed as Eq. (2).

2.7. Kinetic modeling in PHREEQC

For a full description of the kinetic modeling functions in PHREEQC, the readers are referred to the PHREEQC manual (Parkhurst and Appelo, 2013). Here we give a brief introduction relevant to the kinetic library.

In PHREEQC, a kinetic calculation requires two data blocks: KINETICS and RATES. In the KINETICS data block, the user must define the initial moles (in mol kgw ^{1}) and the initial surface area (in m^2 kgw ^{1}, defined in PARM(1)) of the reacting phase. A scaling factor (PARM(2)) is also needed for the calculation, allowing the users to define any coefficients that is needed for the calculation. The rate equation and system-independent parameters, such as rate constants, activation energies, and reaction orders, are defined in the RATES data block. The RATES data block uses BASIC language script to describe the mathematical expression for a particular mineral. The BASIC script for each phase involved in the model simulation must be included in the input or database file prior to use.

We have programmed and assembled a library of these Basic programs for about 100 minerals. An example script for quartz is shown in Fig. 1.

3. BASIC scripts library

The rate equations and parameters in this library can be classified into four categories: (1) Palandri and Kharaka (2004) rate equations; (2) parallel-mechanisms rate equations (e.g. Burch et al., 1993); (3)

Langmuir-adsorption rate equations (e.g. Amram and Ganor, 2005); and (4) other specific rate equations.

3.1. Rate equations in the Palandri and Kharaka format

The rate equation format adopted by Palandri and Kharaka (2004) considered three dissolution mechanisms (acid, neutral, and base) in the following format,

$$r_{net} = S_A \left\{ \begin{array}{c} \left[A_H e^{-E_{a,H}/RT} a_{H^+}^{n_H} \left(1 - \Omega^{p1}\right)^{q1}\right] \\ \left[A_w e^{-E_{a,w}/RT} \left(1 - \Omega^{p2}\right)^{q2}\right] \\ \left[A_{OH} e^{-E_{a,OH}/RT} a_{H^+}^{n_{OH}} \left(1 - \Omega^{p3}\right)^{q3}\right] \end{array} \right\} \quad (12)$$

Only a few minerals in the Palandri and Kharaka (2004) database have p and q values available because most data available were from far-from-equilibrium dissolution experiments. For the minerals without an experimentally determined $f(\Delta_r G)$ term, a $(1-\Omega)$ term was included in all rate equations in the PHREEQC scripts. This additional term ensures that the net reaction rate at equilibrium is always 0 for all rate equations in this library.

For some minerals, new experimental data have become available since Palandri and Kharaka (2004) published their database. The kinetic parameters for these minerals were updated with new parameter values. These phases include 14 minerals by Marty et al. (2015), chlorite (Smith and Carroll, 2016), illite (Smith et al., 2017), kyanite Zhang et al., 2019, lizardite (Daval et al., 2013), and muscovite (Lammers et al., 2017). These publications use a slightly different rate equation from Eq. (9), using a_{OH^-} instead of a_{H+} in the base mechanism (see Eq. (13) and Appendix A).

$$r_{net} = S_A \left\{ \begin{array}{c} \left[A_H e^{-E_{a,H}/RT} a_H^{n_H} \left(1 - \Omega^{p1}\right)^{q1}\right] \\ \left[A_w e^{-E_{a,w}/RT} \left(1 - \Omega^{p2}\right)^{q2}\right] \\ \left[A_{OH} e^{-E_{a,OH}/RT} a_{OH^-}^{n_{OH}} \left(1 - \Omega^{p3}\right)^{q3}\right] \end{array} \right\} \quad (13)$$

3.2. Rate equations involving parallel mechanisms

Burch et al. (1993) measured dissolution rates of albite with pH 8.8 aqueous solution at 80 °C using a continuously stirred flow-through reactor. They found that the dissolution rate at near-equilibrium conditions cannot be described with the relationship in Eqs. (10) and (11). Instead, they used an empirical rate equation which includes two superimposed terms to describe the dissolution rate of albite at near-equilibrium conditions at their experimental pH and T. The rate equation proposed by Burch et al. (1993) is given by

$$r = k_1 S_A \left[1 - e^{-n(|\Delta_r G|/RT)^{m_1}}\right] + k_2 S_A \left[1 - e^{-n(|\Delta_r G|/RT)^{m_2}}\right] \quad (14)$$

where k_1 and k_2 are rate constants were determined from regression, for which the values are 30.46×10^{-12} and 2.73×10^{-12} mol m^{-2} s^{-1}, respectively, at pH = 8.8 and T = 80 °C. The fitted parameters n, m_1, and m_2 are given the values 8.40×10^{-17}, 15.00, and 1.45, respectively.

Hellmann and Tisserand (2006) used the same rate equation as Burch et al. (1993) (Eq. (14)) to fit their albite dissolution data at 150 °C and pH 9.3. The k_1 and k_2 at this pH and T are 1.02×10^{-8} and 1.80×10^{-10}, respectively (mol m^{-2} s^{-1}). The fitted parameters n, m_1, and m_2 are given the values 7.98×10^{-5}, 3.81, and 1.17, respectively.

These two rate equations were fitted from experimental data at specific pH and temperatures. Note that Hellmann and Tisserand (2006) could not fit their experimental data at 150 °C and pH 9.3 using the parameters of Burch et al. (1993), which were based on experimental data at 80 °C and pH 8.8. These rate equations were programmed into BASIC language scripts for minerals. Caution must be exercised for the use of these equations outside of the experimental condition range.

Table 2
Initial conditions for albite hydrolysis calculations.

Parameter	Value or composition
Amount of initial mineral	Albite, 1 mol
Temperature, T	25 °C
Initial pH	6
Surface area, S_A	0.2 m^2 kgw^{-1}
Solution composition, c_i	Ca^{2+}: 0.05 mol kgw^{-1}, Cl^-: 0.08 mol kgw^{-1}, HCO_3^-: 0.02 mol kgw^{-1}
Equilibrium phases	Gibbsite (0 mol), kaolinite (0 mol), paragonite (0 mol), pyrophyllite (0 mol)

3.3. Rate equations in the Langmuir adsorption isotherm format

The Langmuir adsorption isotherm can be used to describe the effects of adsorbed ions on the reactive surface and the dissolution rate (Amram and Ganor, 2005; Lasaga, 1981; Oelkers, 2001). See Marini (2007) for an excellent review. A general form of this type of rate equation is given by Eq. (15).

$$r = S_A k \frac{K_i a_i}{1 + K_i + a_i} \quad (15)$$

For example, the dissolution rate of smectite was studied with a flow-through reactor in acidic solutions (pH 1 to 4.5) at various temperatures (25–70 °C). The following rate equation was used to fit the experimental data (Amram and Ganor, 2005):

$$r = 220 \times e^{\frac{-17600}{RT}} \times \frac{3 \times 10^{-6} \times e^{\frac{10700}{RT}} \times a_{H^+}}{\left(1 + 3 \times 10^{-6} \times e^{\frac{10700}{RT}} \times a_{H^+}\right)} \times S_A \quad (16)$$

This rate equation was programmed into BASIC language scripts for minerals whose data was sourced from these studies.

3.4. Specific rate equations

Rate equations for quartz (with HF added) (Mitra and Rimstidt, 2009), amorphous silica (with HF added) (Mitra and Rimstidt, 2009), quartz (with Na^+ added) (Rimstidt, 2015), amorphous silica (with Na^+ added) (Rimstidt et al., 2016), forsterite (with oxalate added) (Olsen and Rimstidt, 2008), galena (Acero et al., 2007), chalcopyrite (Kimball et al., 2010), montmorillonite (Cappelli et al., 2018), nontronite (Gainey et al., 2014), jarosite (Madden et al., 2012), scorodite (Harvey et al., 2006), and apatite (Harouiya et al., 2007) were collected and programmed into the PHREEQC library. These rate equations were applicable to very specific experimental conditions, such as concentrated organic acid or high salinity solutions.

Besides H^+ and OH^-, other aqueous species can also affect the reaction rate (Bickmore et al., 2008; Rimstidt, 2015; Rimstidt et al., 2016). For example, a rate equation was proposed for quartz dissolution by taking sodium concentration into consideration (Rimstidt, 2015; Rimstidt et al., 2016):

$$J = 0.646\ 10^{-E_{Sa}/2.303RT}) + 6.64\ 10^{-E_{Sa}/2.303RT}) \left(m_{Na^+}^{n_{Na^+}} \Big/ a_{H^+}^{n_{H^+}}\right) \quad (17)$$

where J is the dissolution flux (mol m^{-2} s^{-1}), E_{sa} is the activation energy of the sodium-absent reaction (J mol^{-1}), E_{sc} is the activation energy of the sodium-catalyzed reaction (J mol^{-1}), m_{Na^+} is the molality of Na^+ (mol kgw^{-1}), and n_{Na^+} and n_{H^+} are reaction orders with respect to Na^+ and H^+, respectively. Equation (17) was applicable at 0–50 °C, pH 5.3 to

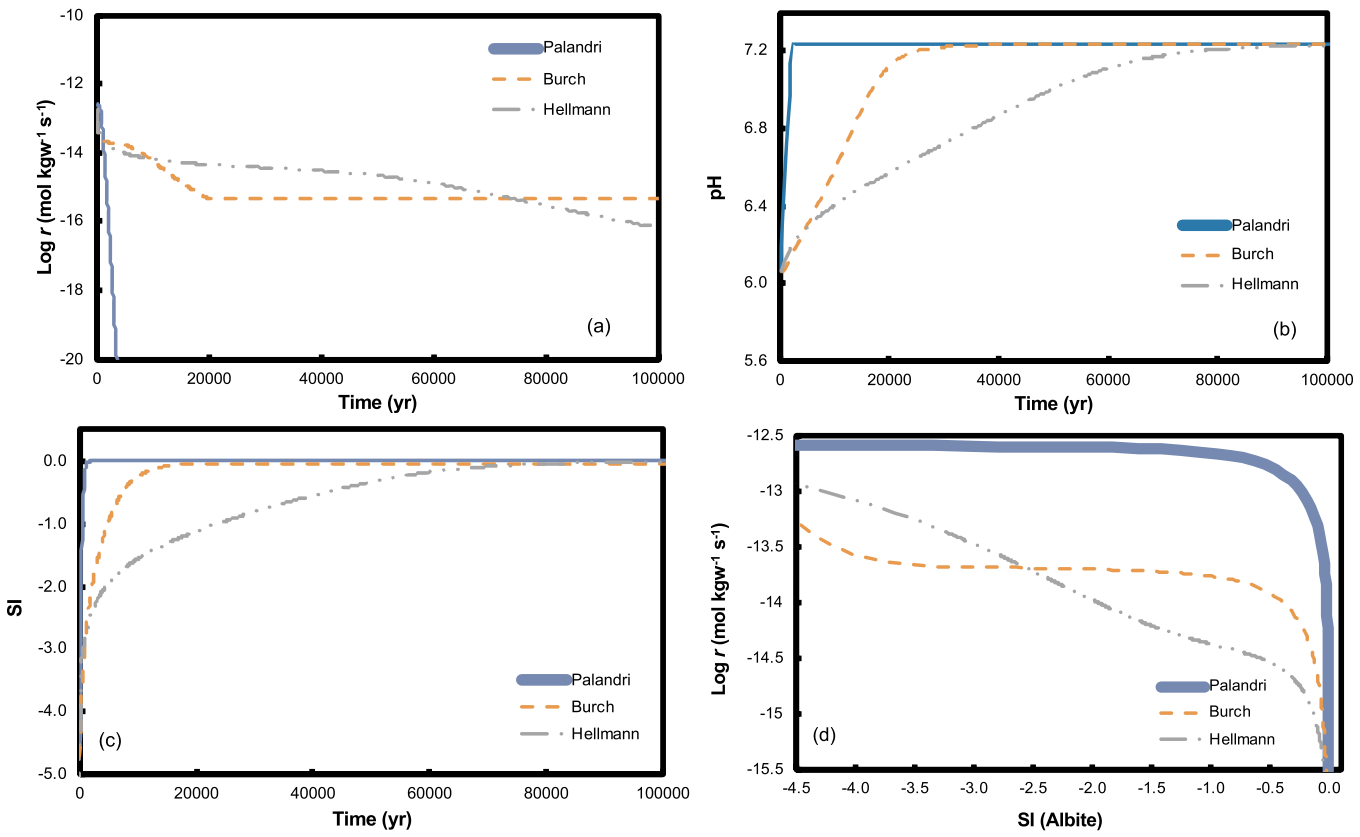

Fig. 2. Comparison of albite hydrolysis reaction paths using three different rate equations. Blue, orange, and grey lines represent simulation results with rate equations of Palandri and Kharaka (2004), Burch et al. (1993), and Hellmann and Tisserand (2006), respectively. (a) albite dissolution rates over time; (b) pH variation over time; (c) saturation indices (SI) of albite over time; (d) dissolution rate vs SI. (For interpretation of the references to colour in this figure legend, the reader is referred to the Web version of this article.)

10.4, and m_{Na} ranging from 0 to 1 mol kgw ^{1}.

4. Example application

To illustrate the utility of the script library, we simulated the reaction path of albite hydrolysis, using BASIC scripts for rate equations of Burch et al. (1993), Hellmann and Tisserand (2006), and Palandri and Kharaka (2004) for albite. The initial conditions for the simulations are the same for the three models and are shown in Table 2. To ensure that only the effect of the $f_{r}G$ function on near-equilibrium rates and reaction path are compared, the rate constants in the three models were normalized to the far-from-equilibrium dissolution rates for albite recommended by Palandri and Kharaka (2004). For simplicity, the secondary phases were assumed to be at equilibrium with the aqueous solution by including the keyword of EQUILIBRIUM_PHASES. Paragonite, kaolinite, gibbsite, and pyrophyllite were allowed to precipitate in the simulation. Equilibrium constants for reactions of aqueous species and minerals were calculated with SUPCRTBL (Zimmer et al., 2016).

For using the Palandri and Kharaka (2004) rate equation (Eq. (12)) to simulate albite hydrolysis, the script block albite in the library was copied and pasted into the PHREEQC input file under keyword RATES. This input file can be found at the journal electronic supplemental materials section with this paper or from the Indiana University web sites noted elsewhere. Note in the library, the Albite script block has the Marty et al. (2015) updated parameters for albite although the rate equation is the same as Palandri and Kharaka (2004). In the same input file, a Kinetics 1 keyword block was also prepared. See the PHREEQC manual for details about this keyword block. The input file can be run with the database *llnl.dat*, which is distributed together with the PHREEQC program from the USGS web site. See the exampela.pqi file for details.

Alternatively, one can use the database *phreeqc-bl-kientics.dat* online (see web address noted elsewhere). This modified database has the kinetic library and relevant phases appended to the *Phreeqc.dat* database. The user only needs to call the Albite RATE block and does not need to be concerned with paragonite because all RATES and PHASES are consistent. See the file example1b.pqi.

To use the Burch et al. (1993) and Hellmann and Tisserand (2006) rate equation (Eq. (14)) for simulating albite hydrolysis is less straightforward. PHREEQC needs the consistency between PHASES and RATES blocks. The program cannot have more than one rate equation for the same phase. In the library, the script for the Burch rate equation is termed Albite(Burch) to differentiate it from the Albite script that uses the Palandri and Kharaka (2004) rate equation. There are two ways to achieve the consistency between RATES and PHASES in this case. The simplest way is to copy the Albite(Burch) script into the input file under RATES and rename it Albite . This will override the Albite script in the database. See the file burch.pqi in the download package. The second way to achieve consistency is to copy the Albite phase entry into the input file and rename Albite as Albite(Burch) .

To make the three rate equation models comparable, we needed to have the same k (k S_A is the far-from-equilibrium rate) for the three models. The k value of Palandri and Kharaka formulation at 25 C and pH 6 was first calculated from Eq. (12) from the parameters for albite in Appendix A (Table 1A, 2A)Table A1 and A2. Then, we forced the sum of k_1 and k_2 in Eq. (14) to be equal to this value with appropriate proportions. The parameters of n, m_1, m_2 in Eq. (14) that represent $f_{r}G$ were retained from those from Burch et al. (1993) and Hellmann and Tisserand (2006). Although developed complicated way to take account

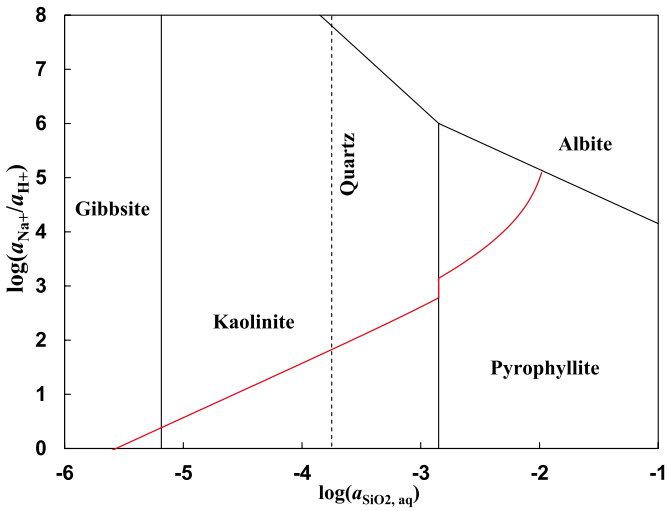

Fig. 3. Two-dimensional activity-activity phase diagram for reaction paths during albite dissolution at 25 C and 1 bar. The red line represents three reaction paths of albite according to rate equations of Palandri and Kharaka (2004), Burch et al. (1993), and Hellmann and Tisserand (2006). The reaction paths are the same and the three lines overlap. (For interpretation of the references to colour in this figure legend, the reader is referred to the Web version of this article.)

of the pH effects on the rates, the solution chemistry only varied from 6 to 7.2, which is within Palandri and Kharaka s neutral pH range. Similar normalization was performed with the Hellmann and Tisserand (2006) parameters (Section 3.2).

The three models produced different results (Fig. 2). Although they started with the same far-from-equilibrium rate by design, albite dissolution rates differed significantly when the aqueous solutions entered the near-equilibrium region because of different r $f(\ _rG)$ functions in the three rate equations. As a result, albite dissolution using the rate equation of Palandri and Kharaka (2004) was the fastest, reaching equilibrium (SI 0.01) within 1800 years at 25 C. The Burch et al. (1993) model reached equilibrium over 17,500 years. The Hellmann and Tisserand (2006) case was the slowest and reached equilibrium after 83,000 years of reaction (Fig. 2).

On the conventional activity-activity diagram, the reaction paths of albite hydrolysis from the three rate equations were identical (Fig. 3). However, the calculated reaction paths in the dissolution process according to the three rate equations are different in the temporal dimension (Fig. 4). After the solution composition quickly crossed the kaolinite-pyrophyllite boundary, the system reached the pyrophyllite stability field, and pyrophyllite is the secondary precipitation phase while albite continues dissolving. As shown the 3-D phase diagram (Fig. 4), the three rate equations gave different predictions on the time needed for the system to reach equilibrium (the boundary between pyrophyllite and albite). As discussed above, the modeling result using Palandri and Kharaka (2004) (red line) was the fastest (about 1800 years); meanwhile, the Hellmann and Tisserand (2006) rate equation (orange line) was the slowest, taking about 83 000 years to reach equilibrium. As the far-from-equilibrium rate in the three cases was

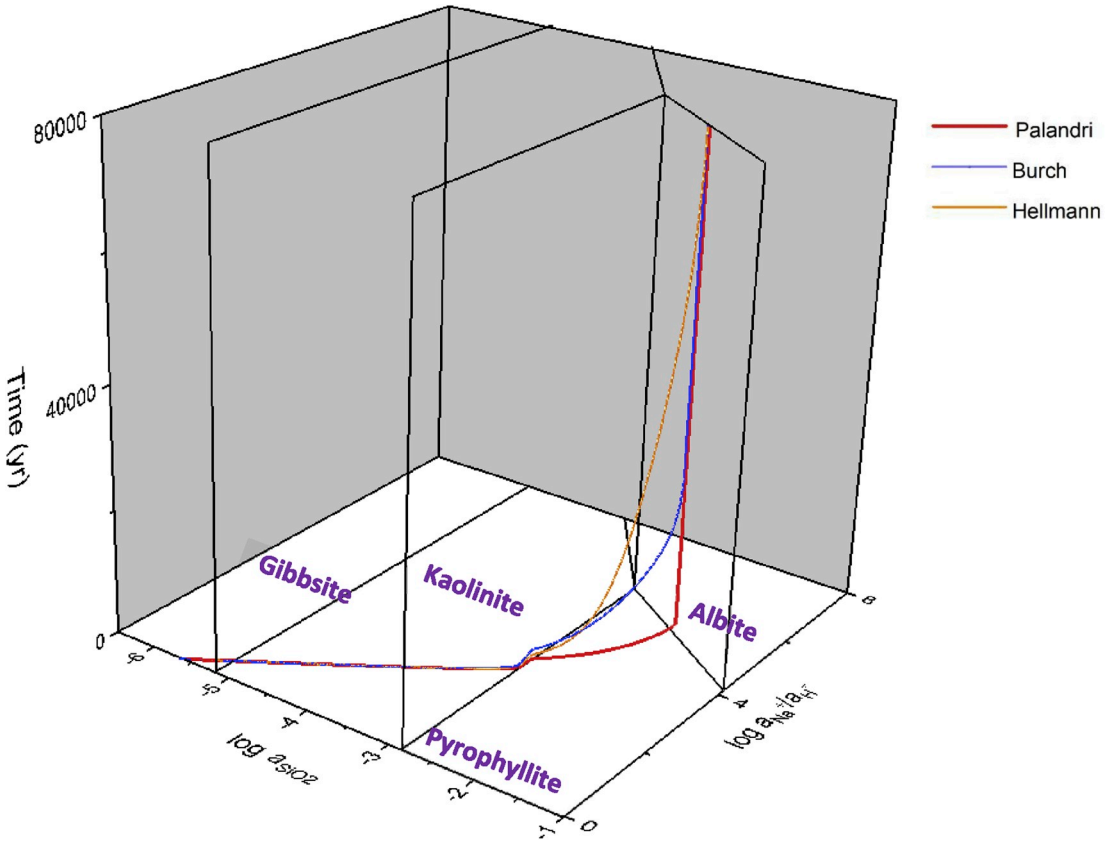

Fig. 4. 3-D activity-activity phase diagram for reaction paths during albite dissolution at 25 C and 1 bar. Red, blue, and orange lines represent reaction paths according to simulations using rate equations of Palandri and Kharaka (2004), Burch et al. (1993), and Hellmann and Tisserand (2006), respectively. (For interpretation of the references to colour in this figure legend, the reader is referred to the Web version of this article.)

fixed at the same level, the different predicted times result from the $f(_rG)$ term, which defines the near-equilibrium rates of albite dissolution reactions.

This example application demonstrated significant effects of the $f(_rG)$ term on dissolution rates. The models all started from the far-from-equilibrium region of the albite-water system. However, all three models proceeded quickly into the near-equilibrium region of the albite-water system after a short periods of time (Fig. 2c). For the remaining simulation time of 100,000 years, albite dissolution proceeded in the near-equilibrium region and the $f(_rG)$ term impacted the dissolution rates (Fig. 2a,d). However, different forms of $f(_rG)$ term led to different projected dissolution rates near-equilibrium (Fig. 2d). Even though the Burch et al. (1993) and Hellmann and Tisserand (2006) rate equations have the same form, the projected rates are different because the parameters in the $f(_rG)$ term are different. The script library of rate equations allowed the users to compare modeling results with different rate equations, and help the users to better evaluate the uncertainties in kinetic modeling studies, regarding the choice of rate equations.

5. Conclusions and remarks

We compiled a library of mineral dissolution rate parameters and equations from the literature and programmed BASIC scripts for the PHREEQC software. About 100 phases are included. Separately, a PHASE file was also developed to be used together with the RATES scripts. PHREEQC requires both data blocks to conduct kinetic modeling. These RATES script blocks and PHASE blocks can be easily copied and pasted into the input files ort append to the PHREEQC databases.

The majority of the rate equations and kinetics parameters in this compilation were derived from far-from-equilibrium dissolution experiments. The relationship between rate and free energy$f_{r}G$ 1 Ω was used as the default expression so that rates go to zero at equilibrium. Scripts without such a provision will lead more user errors because minerals would dissolve in supersaturated solutions. However, as written, the scripts automatically extrapolate dissolution rates at far-from-equilibrium to near-equilibrium conditions, and implicitly assume that precipitation rates can be approximated by reverse of dissolution when the aqueous solution is supersaturated with this phase. Users must be cautious about the limitations of the rate equations and parameters in the library.

We hope this script library will facilitate the application of geochemical kinetics. However, this paper did not evaluate the kinetic rate data; We took the data from the literature and put them into more user-friendly formats. Digital versions of the BASIC scripts can be downloaded for free from https://github.com/HydrogeoIU/PHREEQC-Kinetic-Library and doi.org/10.5967/41gq-yr13. The library of scripts are also included in an online version of PHREEQC, which can be accessed at the corresponding author s Indiana University web site https://hydrogeochem.earth.indiana.edu.

6. Computer code availability

Digital versions of the BASIC scripts, as well as future updates, can be downloaded for free from https://github.com/HydrogeoIU/PHREEQC-Kinetic-Library and doi.org/10.5967/41gq-yr13. The library of scripts are also included in an online version of PHREEQC, which can be accessed at the corresponding author s Indiana University web site www.hydrogeochem.earth.indiana.edu.

Authorship Statement

YZ developed the PHREEQC scripts for kinetics and phases and wrote part of the manuscript.

HB helped in developing the PHREEQC scripts for kinetics and testing the scripts and also wrote part of the manuscript.

YT helped in organizing the script library.

KT developed the online version of PHREEQC and linked to the kinetics library

CZ designed and supervised this project and wrote part of the manuscript.

Acknowledgment

First, we would like to thank David Parkhurst and Tony Appelo for their PHREEQC program and Jim Palandri and Yosef Kharaka for the kinetic database. This work has benefited greatly from discussions with and review by them. We thank all reviewers for their time and their comments have improved the quality and clarity of this paper. CZ acknowledges US NSF grant EAR-19267343. Although the work was partly sponsored by an agency of the United States Government, the views and opinions of authors expressed herein do not necessarily state or reflect those of the United States Government or any agency thereof. This project was also partially funded by the Vice Provost for Research through the Faculty Research Support Program at Indiana University. BH acknowledges support from the China Scholarship Council for the visit of Indiana University as an exchange student. Editing of the manuscript by Anne Hereford and proofreading by Lei Gong is greatly appreciated.

Appendix A. Supplementary data

Supplementary data to this article can be found online at https://doi.org/10.1016/j.cageo.2019.104316.

Appendix A. List of the mineral phases and their kinetic parameters in the PHREEQC library

Table A1
Minerals phases and kinetic parameters in the scripts that uses Eq. (12)

	Acid mechanism				Neutral mechanism			Base mechanism				Other catalyzing species					Ref
	A mol m^{-2} s^{-1}	E_a kJ/mol	n_H	logk_{25}	A mol m^{-2} s^{-1}	E_a kJ/mol	logk_{25}	A mol m^{-2} s^{-1}	E_a kJ/mol	n_H	logk_{25}	Species	A mol m^{-2} s^{-1}	E_a kJ/mol	n_i	logk_{25}	
Almandine	2.18E 11	94.4	1.00	5.20	3.10E 07	103.8	10.70	8.00E-08	37.8	0.35	13.71						1*
Andesine	3.16E 00	53.5	0.54	8.88	3.98E-02	57.5	11.47	1.00E-07	58.5	0.68	17.25						
Andradite	2.18E 11	94.4	1.00	5.20	3.10E 07	103.8	10.70										
Anglesite	7.94E-01	31.3	0.30	5.58	9.53E-02	31.3	6.50										
Anhydrite					2.05E-01	14.3	3.19										
Annite	4.15E-01	49.0	0.67	8.97	9.04E-04	49.0	11.63	3.50E 01	49.0	0.79	7.04						
Anorthite	2.58E-01	16.6	1.41	3.50	1.00E-06	17.8	9.12	1.00E-22	18.1	1.77	25.18						
Anthophyllite	1.00E-03	51.0	0.44	11.94	5.00E-06	51.0	14.24										
As2S3(a)					5.00E-09	8.7	9.83	1.36E-16	8.7	1.21	17.39	O_2			0.18		
Augite	7.00E 06	78.0	0.70	6.82	5.00E 01	78.0	11.97										
Barite	3.09E-02	30.8	0.22	6.90	3.13E-03	30.8	7.90										
Bronzite	9.31E-01	47.2	0.65	8.30	7.53E-01	66.1	11.70										
Brucite	4.00E 05	59.0	0.50	4.73	1.30E-01	42.0	8.24										
Bytownite	1.95E-01	29.3	1.02	5.85	5.01E-05	31.5	9.82	2.51E-16	32.1	1.27	21.22						
Chalcedony					3.47E-02	62.8	12.46										
Chrysotile					1.10E 03	73.2	9.79										
Cordierite	1.11E 16	113.3	1.00	3.80	5.77E-07	28.3	11.20										
Dawsonite					1.01E 04	62.8	7.00										
Diaspore					1.00E-05	47.5	13.33	5.29E-16	47.5	1.50	23.61						
Diopside	3.00E 10	96.1	0.71	6.36	1.00E-04	40.6	11.11										
Dolomite (disordered)	1.47E 06	56.7	0.50	3.76	1.25E 08	95.3	8.60					$P(CO_2)$	4.36E 02	45.7	0.50	5.37	
Dolomite (ordered)	1.34E 03	36.1	0.50	3.19	4.05E 01	52.2	7.53					$P(CO_2)$	9.59E 00	34.8	0.50	5.11	
Enstatite	1.00E 05	80.0	0.60	9.02	2.00E 01	80.0	12.72										
Epidote (ordered)	7.03E 01	71.1	0.34	10.60	2.47E 00	70.7	11.99	3.40E-04	79.1	0.56	17.33						
Fayalite	5.47E 11	94.4	1.00	4.80	1.58E 03	79.0	10.64										
Fluorapatite	1.88E-04	0.0	0.61	3.73	1.00E-08	0.0	8.00										
Fluorite	4.51E 05	73.0	1.00	7.14	1.00E-01	73.0	13.79										
Forsterite	8.38E 04	67.2	0.47	6.85	1.58E 03	79.0	10.64	1.00E-07	56.6	0.60	16.92						
Glauconite	1.21E 10	85.0	0.70	4.80	6.08E 05	85.0	9.10										
Glaucophane	1.92E 09	85.0	0.70	5.60	2.74E 06	94.4	10.10										
Goethite					1.62E 07	86.5	7.94										
Grossular	6.09E 09	85.0	1.00	5.10	3.10E 07	103.8	10.70										
Gypsum					1.64E-03	0.0	2.79										
Halite					1.23E 01	7.4	0.21										
Hematite	1.62E 02	66.2	1.00	9.39	1.90E 04	66.2	7.32										
Hydroxyapatite	5.12E-05	0.0	0.17	4.29	1.00E-06	0.0	6.00										
Ilmenite	1.93E-02	37.9	0.42	8.35	3.00E-05	37.9	11.16										
Jadeite	1.42E 17	132.2	0.70	6.00	1.09E 07	94.4	9.50										
Labradorite	5.01E-01	42.1	0.63	7.67	1.00E-03	45.2	10.91	5.62E-10	46.0	0.78	17.31						
Leucite	1.42E 17	132.2	0.70	6.00	1.07E 04	75.5	9.20	1.82E-01	56.6	0.20	10.66						1*
Lizardite	3.39E 07	75.5	0.80	5.70	3.33E-03	56.6	12.40										
Magnesite	2.51E 06	62.8	1.00	4.60	4.57E 01	62.8	9.34					P (CO2)	6.03E 05	62.8	1.00	5.22	
Magnetite	4.66E-06	18.6	0.28	8.59	3.00E-08	18.6	10.78										
Nepheline	1.99E 08	62.9	1.13	2.73	7.86E 02	65.4	8.56	7.10E-05	37.8	0.20	10.76						
Oligoclase	5.13E 01	65.0	0.46	9.67	2.40E 00	69.8	11.84	5.01E-05	71.0	0.57	16.75						
Paragonite					7.15E-10	22.0	13.00										
Phlogopite					4.82E-08	29.0	12.40										
Prehnite	2.79E 03	80.5	0.26	10.66	1.58E 03	93.4	13.16	3.16E 01	93.4	0.20	17.86						
Pyrite	2.82E 02	56.9	0.50	7.52								O_2	2.64E 05	56.9	0.50	4.55	

(*continued on next page*)

Table A1 (*continued*)

	Acid mechanism				Neutral mechanism			Base mechanism				Other catalyzing species					Ref
	A mol m^{-2} s^{-1}	E_a kJ/mol	n_H	logk_{25}	A mol m^{-2} s^{-1}	E_a kJ/mol	logk_{25}	A mol m^{-2} s^{-1}	E_a kJ/mol	n_H	logk_{25}	Species	A mol m^{-2} s^{-1}	E_a kJ/mol	n_i	logk_{25}	
Pyrophyllite					4.82E-08	29.0	12.40										
Pyrrhotite (hexagonal)	1.78E 04	63.0	0.09	6.79													
Pyrrhotite (monoclinic)	7.29E 00	50.8	0.60	8.04													
Riebeckite	1.67E 02	56.6	0.70	7.70	1.17E-04	47.2	12.20										
SiO2(a)					6.64E 00	74.5	12.24										
Smectite	1.41E-07	23.6	0.34	10.98	2.24E-07	35.0	12.78	6.31E-07	58.9	0.40	16.52						
Spodumene	8.67E 11	94.4	0.70	4.60	1.89E 02	66.1	9.30										
Mg-Staurolite	7.67E-15	37.8	1.00	20.73	5.28E-03	56.6	12.20	2.36E-07	47.2	0.30	14.90						
Talc					2.28E-05	42.0	12.00										
Tourmaline	5.38E 06	75.5	1.00	6.50	4.84E 03	85.0	11.20	2.86E 01	85.0	0.40	13.43						
Tremolite	8.08E-06	18.9	0.70	8.40	8.67E 05	94.4	10.60										
Uraninite					4.33E-03	32.1	7.98										
Wollastonite	1.60E 04	54.7	0.40	5.37	5.00E 00	54.7	8.88										
Zoisite	1.19E 04	66.1	0.50	7.50	1.07E 02	75.5	11.20										
Albite	1.45E 00	58.4	0.34	10.07	4.97E-10	57.0	19.29	7.41E-01	55.5	0.32	9.85						2**
Calcite					6.59E 04	66.0	6.74					HCO_3	1.04E 09	67.0	1.60	2.72	
Celestite	8.13E-01	32.9	0.11	5.85	2.43E-02	34.5	7.66										
Clinochlore (ordered)	7.80E-06	17.0	0.28	8.09	4.07E-14	16.0	16.19	4.39E-06	16.0	0.34	8.16						
CSH(0.8)	6.32E-04	23.0	0.28	7.23	1.71E-14	23.0	17.80										
Cristobalite (high)					7.85E-02	69.0	13.19	2.33E 02	69.0	0.34	9.72						
Dolomite	3.21E 04	46.0	0.61	3.55	2.97E-03	31.0	7.96										
Gibbsite								7.96E 02	48.0	1.00	5.51						
Kaolinite	2.56E-04	43.0	0.51	11.12	5.00E-08	38.0	13.96	2.87E-03	46.0	0.58	10.60						
Microcline	4.59E-06	31.0	0.27	10.77	2.70E-09	31.0	14.00	3.78E-05	31.0	0.35	9.85						
Portlandite	1.10E 10	75.0	0.60	3.10	3.04E 05	75.0	7.66										
Quartz					1.98E 00	77.0	13.19	1.97E 04	80.0	0.34	9.72						
Siderite	3.82E 04	56.0	0.60	5.23	1.36E 01	56.0	8.68										
Montmorillonite	1.53E-01	54.0	0.69	10.28	1.01E-03	63.0	14.03	1.41E-01	61.0	0.34	11.54						
Chlorite_Smith_2016	1.00E-04	30.0	0.74	9.26	4.70E-11	13.0	12.61	1.50E-09	15.0	0.43	11.45						3**
Illite	1.00E-02	58.0	0.55	12.16	2.00E-05	54.0	14.16	1.49E-03	77.0	0.35	16.32						4**
Kyanite					3.83E 00	73.5	12.29										5
Lizardite_Daval_2013	1.23E 05	42.0	0.53	2.27													6
Muscovite	3.00E-03	44.0	0.80	10.23	9.00E-06	45.0	12.93	5.00E-01	61.0	0.60	10.99						7**

[1]Palandri and Kharaka (2004).
[2]Marty et al. (2015).
[3]Smith and Carroll (2016).
[4]Smith et al. (2017).
[5]Zhang et al. (in prep).
[6]Daval et al. (2013).
[7]Lammers et al. (2017).
*The rate of base mechanism in Palandri and Kharaka (2004) uses a_H (see Eq. (8a)).
**The rate of base mechanism in these literature uses a_{OH^-} (see Eq. (8b)).
The rate of acidic mechanism of these phases are also dependent on $a_{Fe^{3+}}$, with $n_{Fe^{3+}}$ 0.50.

Table A2
Minerals phases using other rate equations

Rate equation category	Mineral	Reference
Parallel mechanisms rate equations	Albite_Burch	Burch et al. (1993)
	Albite_Hellmann	Hellmann and Tisserand (2006)
Langmuir adsorption rate equations	Smectite_Amram_2005	Amram and Ganor (2005)
Other specific rate equations	Fluorapatite_Harouiya_2007	Harouiya et al. (2007)
	Chalcopyrite	Kimball et al. (2010)
	Forsterite(ox)	Olsen and Rimstidt (2008)
	Galena	Acero et al. (2007)
	Jarosite	Madden et al. (2012)
	Montmorillonite_Cappelli_2018	Cappelli et al. (2018)
	Nontronite	Gainey et al. (2014)
	Quartz(Na)	Mitra and Rimstidt (2009)
	Quartz(HF)	Rimstidt (2015)
	Scorodite	Harvey et al. (2006)
	SiO2(a)(Na)	Mitra and Rimstidt (2009)
	SiO2(a)(HF)	Rimstidt et al. (2016)

References

Acero, P., Cama, J., Ayora, C., 2007. Rate law for galena dissolution in acidic environment. Chem. Geol. 245, 219 229.

Alekseyev, V.A., Medvedeva, L.S., Prisyagina, N.I., Meshalkin, S.S., Balabin, A.I., 1997. Change in the dissolution rates of alkali feldspars as a result of secondary mineral precipitation and approach to equilibrium. Geochem. Cosmochim. Acta 61, 1125 1142.

Amram, K., Ganor, J., 2005. The combined effect of pH and temperature on smectite dissolution rate under acidic conditions. Geochem. Cosmochim. Acta 69, 2535 2546.

Bickmore, B.R., Wheeler, J.C., Bates, B., Nagy, K.L., Eggett, D.L., 2008. Reaction pathways for quartz dissolution determined by statistical and graphical analysis of macroscopic experimental data. Geochem. Cosmochim. Acta 72, 4521 4536.

Brantley, S.L., Kubicki, J.D., White, A.F., 2008. Kinetics of Water-Rock Interaction. Springer, New York, NY.

Burch, T., Nagy, K., Lasaga, A., 1993. Free energy dependence of albite dissolution kinetics at 80 C and pH 8.8. Chem. Geol. 105, 137 162.

Cappelli, C., Yokoyama, S., Cama, J., Huertas, F.J., 2018. Montmorillonite dissolution kinetics: experimental and reactive transport modeling interpretation. Geochem. Cosmochim. Acta 227, 96 122.

Charlton, S.R., Parkhurst, D.L., 2011. Modules based on the geochemical model PHREEQC for use in scripting and programming languages. Comput. Geosci. 37, 1653 1663.

Daval, D., Hellmann, R., Martinez, I., Gangloff, S., Guyot, F., 2013. Lizardite serpentine dissolution kinetics as a function of pH and temperature, including effects of elevated pCO_2. Chem. Geol. 351, 245 256.

Dobson, P.F., Salah, S., Spycher, N., Sonnenthal, E.L., 2004. Simulation of water rock interaction in the Yellowstone geothermal system using TOUGHREACT. Geothermics 33, 493 502.

Gainey, S., Hausrath, E., Hurowitz, J., Milliken, R., 2014. Nontronite dissolution rates and implications for Mars. Geochem. Cosmochim. Acta 126, 192 211.

Giambalvo, E.R., Steefel, C.I., Fisher, A.T., Rosenberg, N.D., Wheat, C.G., 2002. Effect of fluid-sediment reaction on hydrothermal fluxes of major elements, eastern flank of the Juan de Fuca Ridge. Geochem. Cosmochim. Acta 66, 1739 1757.

Harouiya, N., Chaïrat, C., Köhler, S.J., Gout, R., Oelkers, E.H., 2007. The dissolution kinetics and apparent solubility of natural apatite in closed reactors at temperatures from 5 to 50 ^{o}C and pH from 1 to 6. Chem. Geol. 244, 554 568.

Harvey, M.C., Schreiber, M.E., Rimstidt, J.D., Griffith, M.M., 2006. Scorodite dissolution kinetics: implications for arsenic release. Environ. Sci. Technol. 40 (21), 6709 6714.

Helgeson, H.C., Murphy, W.M., Aagaard, P., 1984. Thermodynamic and kinetic constraints on reaction rates among minerals and aqueous solutions II. Rate constants, effective surface area, and the hydrolysis of feldspar. Geochem. Cosmochim. Acta 48, 2405 2432.

Hellmann, R., Tisserand, D., 2006. Dissolution kinetics as a function of the Gibbs free energy of reaction: an experimental study based on albite feldspar. Geochem. Cosmochim. Acta 70 (2), 364 383.

Jones, G.D., Xiao, Y., 2005. Dolomitization, anhydrite cementation, and porosity evolution in a reflux system: insights from reactive transport models. AAPG Bull. 89, 577 601.

Jones, G.D., Xiao, Y., 2006. Geothermal convection in the Tengiz carbonate platform, Kazakhstan: reactive transport models of diagenesis and reservoir quality. AAPG Bull. 90, 1251 1272.

Kimball, B.E., Rimstidt, J.D., Brantley, S.L., 2010. Chalcopyrite dissolution rate laws. Appl. Geochem. 25 (7), 972 983.

Knauss, K.G., Johnson, J.W., Steefel, C.I., 2005. Evaluation of the impact of CO_2, co-contaminant gas, aqueous fluid and reservoir rock interactions on the geologic sequestration of CO_2. Chem. Geol. 217, 339 350.

Lammers, K., Smith, M.M., Carroll, S.A., 2017. Muscovite dissolution kinetics as a function of pH at elevated temperature. Chem. Geol. 466, 149 158.

Lasaga, A.C., 1981. Rate laws of chemical reactions. In: Lasaga, A.C., Kirkpatrick, R.J. (Eds.), Kinetics of Geochemical Processes, Reviews in Mineralogy 8. Mineralogical Society of America, Washington, D.C., pp. 1 68

Lasaga, A.C., 1995. Fundamental approaches in describing mineral dissolution and precipitation rates. In: White, A.F., Brantley, S.L. (Eds.), Chemical Weathering Rates of Silicate Minerals, Reviews in Mineralogy 31. Mineralogical Society of America, Washington, D.C., pp. 23 86

Lasaga, A.C., 1998. Kinetic Theory in the Earth Sciences. Princeton University Press, Princeton, NJ.

Lasaga, A.C., Soler, J.M., Ganor, J., Burch, T.E., Nagy, K.L., 1994. Chemical weathering rate laws and global geochemical cycles. Geochem. Cosmochim. Acta 58, 2361 2386.

Liu, F., Lu, P., Zhu, C., Xiao, Y., 2011. Coupled reactive flow and transport modeling of CO_2 sequestration in the Mt. Simon sandstone formation, Midwest USA. Int. J. Greenh. Gas Con. 5, 294 307.

Liu, F.Y., Lu, P., Griffith, C., Soong, Y., Hedges, S.W., Hellevang, H., Zhu, C., 2012. CO_2-caprock-brine interaction: reactivity experiments on Eau Claire Shale and a review of literature. Int. J. Greenh. Gas Con. 7, 153 167.

Lu, P., Fu, Q., Seyfried, W.E.J., Hereford, A.G., Zhu, C., 2011. Navajo sandstone-brine-CO_2 interaction: implications for geological carbon sequestration. Environ. Earth Sci. 62, 101 118.

Lu, P., Fu, Q., Seyfried Jr., W.E., Hedges, S.W., Soong, Y., Jones, K., Zhu, C., 2013. Coupled alkali feldspar dissolution and secondary mineral precipitation in batch systems: 2. New Experiments with Supercritical CO_2 and Implications for Carbon Sequestration. Appl. Geochem. 30, 75 90.

Lu, P., Konishi, H., Oelkers, E., Zhu, C., 2015. Coupled alkali feldspar dissolution and secondary mineral precipitation in batch systems: 5. Results of K-feldspar hydrolysis experiments. Chin. J. Geochem. 34, 1 12.

Lu, P., Cantrell, D., 2016. Reactive transport modelling of reflux dolomitization in the Arab-D reservoir, Ghawar field, Saudi Arabia. Sedimentology 63, 865 892.

Madden, M.E., Madden, A., Rimstidt, J., Zahrai, S., Kendall, M., Miller, M., 2012. Jarosite dissolution rates and nanoscale mineralogy. Geochem. Cosmochim. Acta 91, 306 321.

Maher, K., Steefel, C.I., White, A.F., Stonestrom, D.A., 2009. The role of reaction affinity and secondary minerals in regulating chemical weathering rates at the Santa Cruz Soil Chronosequence, California. Geochem. Cosmochim. Acta 73, 2804 2831.

Marini, L., 2007. Geological Sequestration of Carbon Dioxide: Thermodynamics, Kinetics, and Reaction Path Modeling. Elsevier, Amsterdam.

Marty, N.C., Claret, F., Lassin, A., Tremosa, J., Blanc, P., Madé, B., Giffaut, E., Cochepin, B., Tournassat, C., 2015. A database of dissolution and precipitation rates for clay-rocks minerals. Appl. Geochem. 55, 108 118.

Mitra, A., Rimstidt, J.D., 2009. Solubility and dissolution rate of silica in acid fluoride solutions. Geochem. Cosmochim. Acta 73 (23), 7045 7059.

Oelkers, E.H., Schott, J., Devidal, J.L., 1994. The effect of aluminum, pH, and chemical affinity on the rates of aluminosilicate dissolution reactions. Geochem. Cosmochim. Acta 58, 2011 2024.

Oelkers, E.H., 2001. General kinetic description of multioxide silicate mineral and glass dissolution. Geochem. Cosmochim. Acta 65, 3703 3719.

Olsen, A.A., Rimstidt, J.D., 2008. Oxalate-promoted forsterite dissolution at low pH. Geochem. Cosmochim. Acta 72 (7), 1758 1766.

Palandri, J.L., Kharaka, Y.K., 2004. A Compilation of Rate Parameters of Water-Mineral Interaction Kinetics for Application to Geochemical Modeling. Open File Report 2004-1068. U.S. Geological Survey, Menlo Park, CA, p. 64.

Parkhurst, D.L., Appelo, C., 1999. A Computer Program for Speciation, Batch-Reaction, One-Dimensional Transport and Inverse Geochemical Calculations. Water-Resources Investigations Report 99-4259. U.S. Geological Survey, Denver, CO., p. 312

Parkhurst, D.L., Appelo, C., 2013. Description of Input and Examples for PHREEQC Version 3–A Computer Program for Speciation, Batch-Reaction, One-Dimensional Transport, and Inverse Geochemical Calculations. Techniques and Methods, 6-A43. U.S. Geological Survey, Reston, VA., p. 497

Pham, V.T.H., Lu, P., Aagaard, P., Zhu, C., Hellevang, H., 2011. On the potential of CO_2 water rock interactions for CO_2 storage using a modified kinetic model. Int. J. Greenh. Gas Con. 5, 1002 1015.

Plummer, L.N., Wigley, T.M.L., Parkhurst, D.L., 1978. The kinetics of calcite dissolution in CO_2-water systems at 5 to 60 ^{o}C and 0.0 to 1.0 atm CO_2. Am. J. Sci. 278, 179 216.

Perez-Fodich, A., Derry, L.A., 2019. Organic acids and high soil CO_2 drive intense chemical weathering of Hawaiian basalts: insights from reactive transport models. Geochem. Cosmochim. Acta 249, 173 198.

Rimstidt, J.D., 2014. Geochemical Rate Models: an Introduction to Geochemical Kinetics. Cambridge University Press, Cambridge, UK.

Rimstidt, J.D., 2015. Rate equations for sodium catalyzed quartz dissolution. Geochem. Cosmochim. Acta 167, 195 204.

Rimstidt, J.D., Zhang, Y., Zhu, C., 2016. Rate equations for sodium catalyzed amorphous silica dissolution. Geochem. Cosmochim. Acta 195, 120 125.

Roy, M., Martin, J.B., Smith, C.G., Cable, J.E., 2011. Reactive-transport modeling of iron diagenesis and associated organic carbon remineralization in a Florida (USA) subterranean estuary. Earth Planet. Sci. Lett. 304, 191 201.

Schott, J., Pokrovsky, O.S., Oelkers, E.H., 2009. The link between mineral dissolution/precipitation kinetics and solution chemistry. Rev. Mineral. Geochem. 70, 207 258.

Steefel, C.I., Yabusaki, S.B., Mayer, K.U., 2015. Reactive transport benchmarks for subsurface environmental simulation. Comput. Geosci. 19, 439 443.

Smith, M.M., Carroll, S.A., 2016. Chlorite dissolution kinetics at pH 3 10 and temperature to 275 C. Chem. Geol. 421, 55 64.

Smith, M.M., Dai, Z., Carroll, S.A., 2017. Illite dissolution kinetics from 100 to 280 C and pH 3 to 9. Geochem. Cosmochim. Acta 209, 9 23.

Spycher, N.F., Sonnenthal, E.L., Apps, J.A., 2003. Fluid flow and reactive transport around potential nuclear waste emplacement tunnels at Yucca Mountain, Nevada. J. Contam. Hydrol. 62 63, 653 673.

Stumm, W., 1992. In: Chemistry of Solid-Water Interfaces: Processes at the Mineral-Water and Particle-Water Interface in Natural Systems, first ed. John Wiley & Sons, New York.

Tutolo, B.M., Kong, X.Z., Seyfried, W.E., Saar, M.O., 2015. High performance reactive transport simulations examining the effects of thermal, hydraulic, and chemical (THC) gradients on fluid injectivity at carbonate CCUS reservoir scales. Int. J. Greenh. Gas Con. 39, 285 301.

Wanner, C., Peiffer, L., Sonnenthal, E., Spycher, N., Iovenitti, J., Kennedy, B.M., 2014. Reactive transport modeling of the Dixie Valley geothermal area: insights on flow and geothermometry. Geothermics 51, 130 141.

Whitaker, F.F., Xiao, Y., 2010. Reactive transport modeling of early burial dolomitization of carbonate platforms by geothermal convection. AAPG Bull. 94, 889 917.

White, S.P., Allis, R.G., Moore, J., Chidsey, T., Morgan, C., Gwynn, W., Adams, M., 2005. Simulation of reactive transport of injected CO_2 on the Colorado Plateau, Utah, USA. Chem. Geol. 217, 387 405.

Wilkin, R.T., DiGiulio, D.C., 2010. Geochemical impacts to groundwater from geologic carbon sequestration: controls on pH and inorganic carbon concentrations from reaction path and kinetic modeling. Environ. Earth Sci. 44, 4821 4827.

Wolery, T.J., 1992. EQ3/6: Software Package for Geochemical Modeling of Aqueous Systems: Package Overview and Installation Guide. Lawrence Livermore National Laboratory Report UCRL-MA-110662 PT I, Livermore, CA version 8.0.

Xu, T., Apps, J.A., Pruess, K., Yamamoto, H., 2007. Numerical modeling of injection and mineral trapping of CO_2 with H_2S and SO_2 in a sandstone formation. Chem. Geol. 242, 319 346.

Xu, T., Kharaka, Y.K., Doughty, C., Freifeld, B.M., Daley, T.M., 2010. Reactive transport modeling to study changes in water chemistry induced by CO_2 injection at the Frio-I Brine Pilot. Chem. Geol. 271, 153 164.

Xu, T., Ontoy, Y., Molling, P., Spycher, N., Parini, M., Pruess, K., 2004. Reactive transport modeling of injection well scaling and acidizing at Tiwi field, Philippines. Geothermics 33, 477 491.

Xu, T., Pruess, K., 2001. On fluid flow and mineral alteration in fractured caprock of magmatic hydrothermal systems. J. Geophys. Res.-Sol. Ea. 106, 2121 2138.

Xu, T., Sonnenthal, E., Spycher, N., Pruess, K., 2006. TOUGHREACT a simulation program for non-isothermal multiphase reactive geochemical transport in variably saturated geologic media: applications to geothermal injectivity and CO_2 geological sequestration. Comput. Geosci. 32, 145 165.

Xu, T., Spycher, N., Sonnenthal, E., Zhang, G., Zheng, L., Pruess, K., 2011. TOUGHREACT Version 2.0: a simulator for subsurface reactive transport under non-isothermal multiphase flow conditions. Comput. Geosci. 37, 763 774.

Zimmer, K., Zhang, Y., Lu, P., Chen, Y., Zhang, G., Dalkilic, M., Zhu, C., 2016. SUPCRTBL: a revised and extended thermodynamic dataset and software package of SUPCRT92. Comput. Geosci. 90, 97 111.

Zhang, G., Lu, P., Wei, X., Zhu, C., 2016. Impacts of mineral reaction kinetics and regional groundwater flow on long-term CO_2 fate at sleipner. Energy Fuel. 30, 4159 4180.

Zhang, L., Soong, Y., Dilmore, R., Lopano, C., 2015. Numerical simulation of porosity and permeability evolution of Mount Simon sandstone under geological carbon sequestration conditions. Chem. Geol. 403, 1 12.

Zhang, S., DePaolo, D.J., Xu, T., Zheng, L., 2013. Mineralization of carbon dioxide sequestered in volcanogenic sandstone reservoir rocks. Int. J. Greenh. Gas Con. 18, 315 328.

Zhu, C., 2009. Geochemical modeling of reaction paths and geochemical reaction networks. Rev. Mineral. Geochem. 70, 533 569.

Zhu, C., Anderson, G.M., 2002. Environmental Applications of Geochemical Modeling. Cambridge University Press, Cambridge, UK, pp. 230 237.

Zhu, C., Lu, P., Zheng, Z., Ganor, J., 2010. Coupled alkali feldspar dissolution and secondary mineral precipitation in batch systems: 4. Numerical modeling of kinetic reaction paths. Geochem. Cosmochim. Acta 74, 3963 3983.

Zhang, Y., Rimstidt, D.J., Huang, Y., Zhu, C., 2019. Kyanite Far from Equilibrium Dissolution Rate at 0 22 oC and pH of 3.5~7.5. 38, pp. 472 480.